ChemComm

Accepted Manuscript

This article can be cited before page numbers have been issued, to do this please use: J. Bae, K. Baek, D. Yuan, W. Kim, K. Kim, H. Zhou and J. Park, *Chem. Commun.*, 2017, DOI: 10.1039/C7CC04799A.

ROYAL SOCIETY OF CHEMISTRY

rsc.li/chemcomm

View Article Online
DOI: 10.1039/C7CC04799A

Chemical Communications

COMMUNICATION

Reversible Photoreduction of Cu(II)-Coumarin Metal-Organic Polyhedra

Jaeyeon Bae,[a] Kangkyun Baek,[b] Daqiang Yuan,[c] Wooram Kim,[b,d] Kimoon Kim,[b,d] Hong-Cai Zhou,[e] and Jinhee Park[a]*

Received 00th January 20xx,
Accepted 00th January 20xx

DOI: 10.1039/x0xx00000x

www.rsc.org/

We report a new approach for photoinduced reduction of Cu^{2+} that will enrich the structural diversity of coordination complexes and be a valuable contributor to the development of Cu^{+}/Cu^{0}-based catalysts. To realize controlled Cu^{2+} reduction, coumarin as a triplet quencher of excited benzophenone was tethered to Cu(II)-metal-organic polyhedra (MOPs). The photoinduced catalytic activity of the Coumarin-MOPs was also examined in a Cu(I)-catalyzed azide-alkyne cycloaddition (CuAAC).

Metal-organic polyhedra (MOPs) are discrete cage-like supramolecules that have been studied extensively owing to their designability, tailorability, solubility, and intrinsic porosity.[1-8] Previously, various structural MOPs inspired by geometric entities such as Platonic and Archimedean solids were extensively reported.[3-5, 8, 9] Recent research has focused on the development of functional MOP materials based on direct self-assembly, post-synthetic modification[10-12], and assembly with other materials[13-16] for applications in guest molecule storage,[17] separation,[18, 19] catalysis,[20] drug delivery,[21, 22] sensing,[14, 23-25] etc.[26, 27] In particular, post-synthetic modifications have been used to attach additional functional groups to organic linkers that are not compatible with typical MOP syntheses.[28, 29] However, the study of MOPs as stimuli-responsive materials remains in the early stages, and optically responsive MOPs, in particular, have rarely been reported. For example, a diaryl ethane-based cage-like molecule showed photoinduced guest molecule capture and release, which was caused by changes in its rigidity during the electrocyclization and cycloreversion reactions of the ligand.[30] Park *et al.* demonstrated an optically responsive solubility change of an azobenzene-functionalized MOP through *trans-cis* isomerization.[31]

In this report, cuboctahedral MOPs bearing Cu-paddlewheel clusters were employed to realize the controlled photoinduced reduction of Cu^{2+}. Since the organic ligands are located close to the Cu-paddlewheel clusters in the MOPs, a reversible and controlled Cu^{2+} reduction was accomplished through judicious ligand design. As a triplet photosensitizer, benzophenone facilitates the reduction of Cu^{2+} to Cu^{+} and then to Cu^{0}. Coumarin ides an effective triplet quencher of excited benzophenone due to the relatively low $^{3}\pi,\pi^{*}$ transition energy of coumarin compared with that of benzophenone.[32] Thus, coumarin-modified MOPs (Coumarin-MOPs) can control Cu^{2+} reduction via energy transfer from benzophenone to coumarin. Generally, a Cu^{+} oxidation state is difficult to maintain due to its high reduction potential. However, Coumarin-MOPs stabilize the Cu^{+} state by perturbing the direct electron transfer from benzophenone to Cu^{2+} and Cu^{+}. Notably, Cu^{+} states with long lifetimes allow their catalytic activity to be tested. In general, such a photoinduced reduction system is useful because experiments can be designed with a stable Cu^{2+} pre-catalyst; light irradiation then initiates the catalytic activity easily and on demand. The catalytic activity of the reduced Cu^{+} state was examined in the Cu(I)-catalyzed azide-alkyne cycloaddition (CuAAC).[33, 34]

As zero-dimensional materials, MOPs are easily dispersed in solvents through the proper choice of organic linkers and solvents. This differentiates MOPs from their 3-dimensional analogues, i.e. metal-organic frameworks (MOFs) and porous coordination polymers (PCPs).[35] In this report, the coumarin groups in MOPs act not only as the triplet quencher but also as a solubility enhancer. Cu^{2+} salts and MOPs in organic solvents such as *N*,*N*-dimethylformamide (DMF) and *N*,*N*-dimethylacetamide (DMAc) becomes insoluble when Cu^{2+} is reduced to Cu^{+}. Once MOPs are aggregated, only the surface exposed to the photosensitizer undergoes photoinduced reduction, and only the surface exposed to air may be re-oxidized. Therefore, maintaining high solubility is a prerequisite for the reversible redox reaction of Cu^{2+} complexes. The coumarin moieties allow the MOPs to be soluble during the redox processes, leading to reversible and homogeneous transformations.

Inspired by typical cuboctahedral MOP synthetic protocols, three isophthalate-based ligands (**L1**, **L2**, and **L3**) were prepared in three steps using dibromoalkane, 7-hydroxyl coumarin, and dimethyl 5-

---

[a] Department of Emerging Materials Science, Daegu Gyeongbuk Institute of Science and Technology, Daegu 42988, Republic of Korea. E-mail: jinhee@dgist.ac.kr
[b] Center for Self-assembly and Complexity, Institute for Basic Science, Pohang 37673, Republic of Korea
[c] State Key Lab of Structure Chemistry, Fujian Institute of Research on the Structure of Matter, Chinese Academy of Sciences, Fuzhou, 350002, China
[d] Department of Chemistry, Pohang University of Science and Technology, Pohang 37673, Republic of Korea,
[e] Department of Chemistry, Texas A&M University, PO Box 30012, College Station, TX 77842-3012, USA

Electronic Supplementary Information (ESI) available: Experimental details, supporting figures and graphs, and crystallographic data tables. See DOI: 10.1039/x0xx00000x

View Article Online
DOI: 10.1039/C7CC04799A

hydroxyisophthalate (See the Supplementary Information for the structures and synthetic procedure for **L1**, **L2**, and **L3**). Three different dibromoalkanes (i.e., dibromoethane (for **L1**), dibromopropane (for **L2**), and dibromohexane (for **L3**)) were used to control the distance between coumarin and the Cu-paddlewheel clusters (Figures 1c and S5) because we initially hypothesized that this distance determines the reduction rate. For clarity, the MOPs derived by **L1**, **L2**, and **L3** were named as Coumarin-MOP-1, Coumarin-MOP-2, and Coumarin-MOP-3, respectively. The optically inert MOP-4 was also prepared with *tert*-butyl isophthalate and Cu^{2+} according to a previous report.[11] Coumarin-MOP-1, which consists of the least flexible ligand, crystallized into a blue, block-shaped crystal via ether vaporization, and its structure was unambiguously determined by single-crystal X-ray diffraction measurements. Twenty-four coumarin groups dangled from the cuboctahedral cage of Coumarin-MOP-1 (Figure 1a). The structures of Coumarin-MOP-2 and Coumarin-MOP-3 are analogues of Coumarin-MOP-1 in that the coumarins were tethered to the cuboctahedral cages through flexible propane and hexane moieties, respectively (Figures 1b and S5).[15, 36, 37] However, Coumarin-MOP-2 and -3 did not crystallize into large crystals presumably due to the considerable flexibility of **L2** and **L3**. In addition, MOP crystals generally include large amounts of solvent among the cages. Thus, single-crystal diffraction analyses of Coumarin-MOP-2 and Coumarin-MOP-3 were not possible. Nevertheless, atomic force microscopy (AFM) analysis of those Coumarin-MOP-2 and -3 confirms the formation of cage-like particles with 3–4 nm sizes (Figures 2e-f and S6-8).[29] The simulated structures of Coumarin-MOP-2 and Coumarin-MOP-3 were shown in Figure 1b and S5. The Based on the crystallographic data and excluding the alkyl coumarin groups, the cuboctahedral cage is ~2.1 nm. Because all Coumarin-MOPs include the same cuboctahedral cage, the overall sizes of the MOPs as measured from one coumarin to the other on the opposite side in the crystal and simulated structures can be directly related with the distance between coumarin and the Cu-paddlewheel clusters. In addition, not only the calculated sizes from the crystalline and simulated structures but also the measured sizes from the AFM and dynamic light scattering (DLS) data are critical as direct evidence to prove the relationship between the distance and the reduction rate (Figure S9). The MOP sizes from the above-mentioned methods were added to Table S2. From the AFM images and DLS data, Coumarin-MOP-3 is 0.5-0.6 nm larger overall than Coumarin-MOP-1 and -2, and the sizes of Coumarin-MOP-1 and -2 are similar size.

Controlled photoinduced reduction of Cu^{2+} was demonstrated in the Coumarin-MOPs. First, the Coumarin-MOPs were dissolved in DMF and methanol for their efficient hydrogen donating and electron transfer properties. Adding diethyl ether to the solution moderated the solubility change during the Cu^{2+} reduction process. The ratio of DMF, methanol, and diethyl ether in the solution was 9:0.5:0.5, which was optimized for the reversible reduction and oxidation process. Moles of benzophenone equivalent to those of Cu^{2+} of the Coumarin-MOPs were added to the MOP solutions. All MOP reduction experiments were conducted under inert conditions with 365 nm UV irradiation. Additional experimental details are described in the Supplementary Information. Reduction of all Coumarin-MOPs was monitored not only by eye observation but also by UV-Vis spectroscopy. The blue colour (absorption λ_{max}= 720 nm) of the MOP-solutions faded upon Cu^{2+} to Cu^{+} reduction, because of the absence of *d-d* transitions in Cu^{+} (d^{10}) (Figures 1d-e and S18-23). Further, the new absorption band at 563 nm, which indicates Cu nanoparticle formation (Figures 1f and S18-23), confirms the reduction of Cu^{+} to Cu^{0}. As a control experiment, the reductions of $Cu(CH_3COO)_2$ and MOP-4 were irreversible and uncontrollable (Figure S24-25). The irreversible process is mainly caused by the formation of precipitates during the reduction from Cu^{2+} to $Cu^{+/0}$.

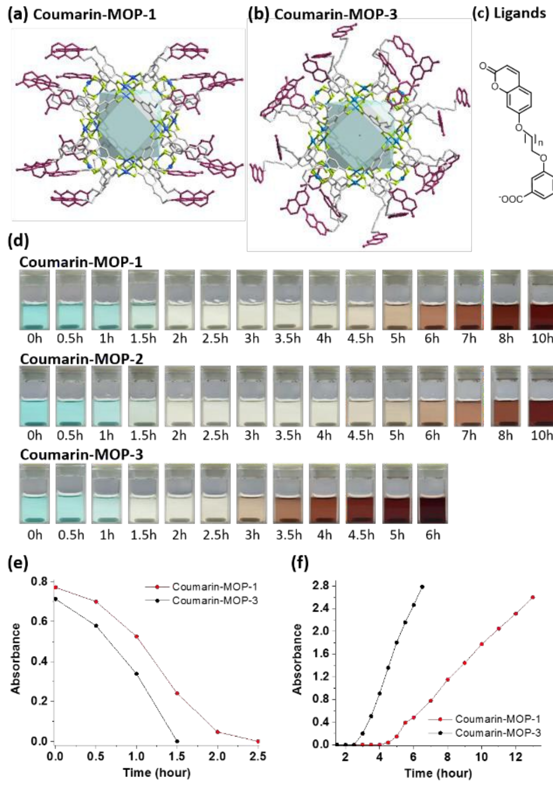

Figure 1. Crystal structure of Coumarin-MOP-1 (a) and simulated structure of Coumarin-MOP-3 (b). (c) Ligand structures: n=1, 2, and 5 for **L1**, **L2**, and **L3**, respectively. (d) Photographs of Coumarin-MOP-1, Coumarin-MOP-2, and Coumarin-MOP-3 during the Cu^{2+} to Cu^{0} photoinduced reduction process. The hours indicate the UV irradiation time. (e) Absorbance change at 720 nm for Cu^{2+} to Cu^{+} reduction for Coumarin-MOP-1 and -3. (f) Absorbance change at 563 nm for Cu^{+} to Cu^{0} reduction for Coumarin-MOP-1 and -3.

A proposed mechanism for the sequential reduction of Cu^{2+} to Cu^{+} and then to Cu^{0} is given in Reactions [1]–[5].[32, 38, 39] Photoabsorption generates benzophenone in the n,π* triplet state. Subsequently, the radical-like benzophenone in the n,π* triplet state abstracts a hydrogen atom from methanol or ether, generating reactive radical pairs [1]. The benzophenone radical then donates the electron to Cu^{2+}, and a proton is transferred to solvent or the acetate remaining in solution [2]. When the Cu^{+} is exposed to oxygen in air, one electron is transferred from Cu^{+} to O_2 [3], followed by the reduction of the oxidized solvent [4].

[1] $BP + Solvent + h\nu \longrightarrow BP\text{-}H^{\cdot} + Solvent^{\cdot}$
[2] $BP\text{-}H^{\cdot} + Cu^{2+} + CH_3COO^{-}/Solvent^{\cdot} \longrightarrow [BP...Cu^{+}] + CH_3COOH/Solvent^{\cdot+}$
[3] $O_2 + Cu^{+} \longrightarrow O_2^{\cdot-} + Cu^{2+}$
[4] $O_2^{\cdot-} + Solvent^{\cdot+} \longrightarrow O_2 + Solvent$
[5] $BP + Coumarin + h\nu \longrightarrow BP^{*} + Coumarin \longrightarrow BP + Coumarin^{*}$

For the two-electron reduction from Cu^{2+} to Cu^{0}, [1] and [2] must be repeated with Cu^{+} instead of Cu^{2+}. This proposed mechanism explains the two-electron reduction of Cu^{2+} with one equivalent of

View Article Online
DOI: 10.1039/C7CC04799A

benzophenone. The reduction of Cu^{2+} to Cu^{+} in MOP-4 took less than 30 min under the same UV irradiation conditions, followed by the reduction of Cu^{+} to Cu^{0} (Figure S24). This uncontrollable reduction process is not suitable to isolate the Cu^{+} state for practical use. Reaction [5] illustrates the energy transfer from benzophenone to coumarin as an alternative step for excited-state benzophenone. Excitation of coumarin with benzophenone is almost 10 times faster than that of coumarin itself, as shown in the UV-Vis spectra (Figures S15 and S16), indicating that coumarin can accept energy from benzophenone. When coumarin was not tethered to the MOPs, the reduction was not successful due to the rapid formation of precipitates (Figure S26). In contrast, when coumarin was tethered to the MOPs through the alkyl groups the reduction rates were significantly attenuated, and even controlled by changing the distance between coumarin and the Cu-paddlewheel clusters. 1.125 mM Coumarin-MOP-1, -2, and -3 were reduced from Cu^{2+} to Cu^{+} within 2.5, 2.0, and 1.5 h, respectively (Figures 1d-e and S18-23). Notably, the Cu^{+} states in Coumarin-MOPs lasted for 1.5~2 h, which is long enough to isolate the Cu^{+} state, even during continuous UV irradiation. These results indicate that the energy transfer from excited-state benzophenone to coumarin notably delays the Cu^{+} reduction process. We note that even the use of one-quarter equivalent benzophenone relative to Cu^{2+} resulted in the similar lifetime of the Cu^{+} state (Figure S27). Further, it is noteworthy that even though Cu^{+} leaching from the MOP structures cannot be prevented, the Cu^{+} state persisted for at least 1 month after the UV irradiation was stopped (Figure S33).

The Cu^{+} to Cu^{0} reduction of Coumarin-MOP-1 and -2 did not show any significant rate difference, indicating that coumarin in both MOPs can equally deactivate the excited-state benzophenone coordinated to Cu^{+} (Figure S18-21). However, the Cu^{+} to Cu^{0} reduction for Coumarin-MOP-1 and -3 took 8.5 and 3 h, respectively, to reach an absorbance of 2 (Figure 1f). The absorbance at 563 nm of Coumarin-MOP-1 after 13 h of UV exposure was even lower than that of Coumarin-MOP-3 after 6.5 h of UV exposure (Figure 1f). This substantial rate difference is indirectly indicative of the benzophenone coordination to the Cu^{+} clusters following electron transfer. The coumarin group is close to benzophenone in Coumarin-MOP-1 and -2. Thus, it appears as though electron transfer from excited-state benzophenone to Cu^{+} is perturbed more effectively by the energy transfer from excited-state benzophenone to coumarin (Reaction [5]). In fact, reduction of Cu^{+} to Cu^{0} generated Cu nanoparticles, as evidenced by blue-shifted absorption bands upon extended UV irradiation time (Figure S18–23). Notably, their solubility was retained without any visible precipitates. Owing to the rapid oxidation of the Cu^{+}-MOPs and Cu nanoparticles to Cu^{2+} upon air exposure, the further analysis such as X-ray photoelectron spectroscopy (XPS) and scanning electron microscopy (SEM) was not possible. Additionally, this Cu nanoparticle formation caused the irreversible reduction and oxidation of the Cu-paddlewheels because the bonds between Cu and the ligands broke (Figure 2d).

The Cu^{2+} and Cu^{+} states in the Coumarin-MOPs were reversible upon alternating the UV irradiation and O_2 exposure in three cycles (Figures 2a-c and S30-32). AFM images of the Coumarin-MOPs after three cycles (one cycle: $Cu^{2+} \rightarrow Cu^{+} \rightarrow Cu^{2+}$) showed sphere-like MOPs (Figures 2e-f and S6–8). There is no significant size difference before or after the Cu^{2+} to Cu^{+} reduction process. The weak coordination bond of the paddlewheel clusters with $Cu^{+/0}$ leads to limited reversibility, indicating the structural collapse of the $Cu^{+/0}$-MOPs.

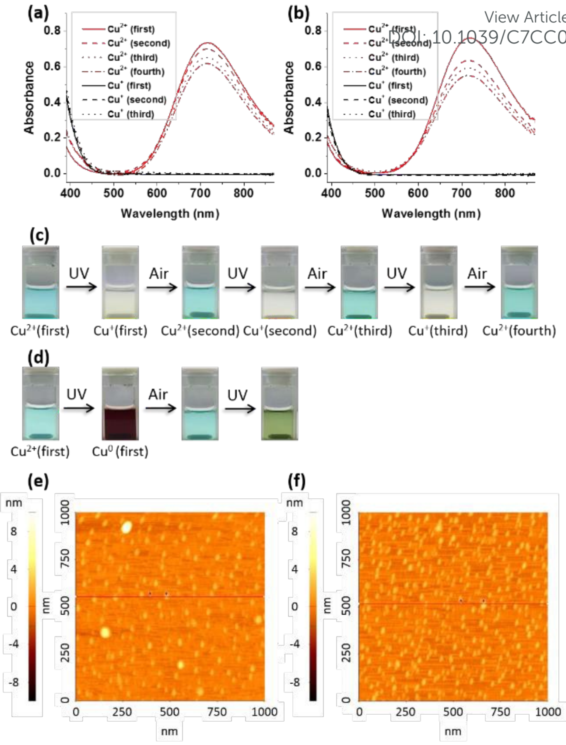

Figure 2. UV-vis spectra during the reversible reduction and oxidation processes of Coumarin-MOP-1 (a) and Coumarin-MOP-2 (b). Monitoring of colour change during the c) reversible reduction and oxidation processes for Coumarin-MOP-3 and d) irreversible reduction and oxidation processes for Coumarin-MOP-3. AFM images of Coumarin-MOP-3 before (e) and after the Cu^{2+} to Cu^{+} reduction process (f).

The reduction system developed herein has been utilized in the CuAAC as a photoinduced homogeneous catalyst. The photoinduced catalytic activities reported previously are mainly based on photodissociation processes or electron transfer from the coordinated benzophenone to Cu^{2+}.[38, 40] Previous reaction systems did not consider strategic molecular design to control the reduction kinetics or to retain the relatively unstable Cu^{+} states. As a model reaction to probe the catalytic activity of the Cu^{+} states, the cycloaddition reaction between phenylacetylene and phenyl azide was selected. Based on the reduction time from Cu^{2+} to Cu^{+} with Coumarin-MOP-1, a solution of phenylacetylene, phenyl azide, Coumarin-MOP-1 (5 mol%), and benzophenone was irradiated by UV light at 365 nm for 3 h (Scheme 1). The reaction was continued for an additional 3 h without irradiation for its completion. 1,4-Disubstituted 1,2,3-triazole was isolated as a crystalline precipitate with 89% yield and analyzed by NMR spectroscopy. Under identical reaction conditions, the reaction with CuI and CuCl as traditional catalysts exhibited low yields of 47 % and 33%, respectively. We assume that the low conversion rates resulted from the low solubility of CuI and CuCl in the solution compared to Coumarin-MOP-1.[41] The detailed experimental procedures are described in Supporting Information-Part S6. Overall, this result demonstrates the potential application of a MOP as a photoinduced catalyst, which has been seldom explored.

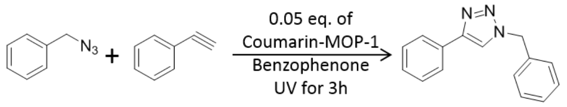

Scheme 1. Cu(I)-Catalyzed Azide-Alkyne Cycloaddition (CuAAC).

We have developed a photoinduced Cu^{2+} to Cu^{+}/Cu^{0} reduction system by employing Cu-cuboctahedral MOPs. The MOPs are ideal compounds to study photoinduced Cu^{2+} reduction processes because desired functional groups can be introduced relatively easily into the system. The MOPs were functionalized by the triplet quencher coumarin, yielding a relatively long lifetime of the Cu^{+} states, even during continuous UV irradiation. The distance between the benzophenone coordinated to Cu^{+} and coumarin was manipulated by changing the length of the alkyl groups on the organic linkers. When the distance is less, Cu^{+} reduction is significantly delayed due to an efficient transfer of energy from benzophenone to coumarin. The reduction and oxidation between the Cu^{2+} and Cu^{+} oxidation states in the Coumarin-MOPs were reversible by alternating UV irradiation and air exposure, presumably until the MOP structures became degraded. Finally, we successfully applied the Coumarin-MOP photoinduced catalysts to the CuAAC. Stabilizing the Cu^{+}-MOPs and Cu^{0} nanoparticles generated by the process developed in this report are currently being explored.

This work was partly supported by the National Research Foundation of Korea (NRF) and grants funded by the Korean government (Nos. NRF-2016R1C1B2009987 and NRF-2016M2B2A9912217). J. Park thanks the support from the Faculty Start-up Fund (2017010035) of the Daegu Gyeongbuk Institute of Science and Technology (DGIST).

References

1. N. Ahmad, A. H. Chughtai, H. A. Younus and F. Verpoort, *Coord. Chem. Rev.*, 2014, **280**, 1-27.
2. M. Han, D. M. Engelhard and G. H. Clever, *Chem. Soc. Rev.*, 2014, **43**, 1848-1860.
3. Z. Lu, C. B. Knobler, H. Furukawa, B. Wang, G. Liu and O. M. Yaghi, *J. Am. Chem. Soc.*, 2009, **131**, 12532-12533.
4. J.-R. Li, A. A. Yakovenko, W. Lu, D. J. Timmons, W. Zhuang, D. Yuan and H.-C. Zhou, *J. Am. Chem. Soc.*, 2010, **132**, 17599-17610.
5. Y.-T. Zhang, X.-L. Wang, S.-B. Li, Y.-R. Gong, B.-Q. Song, K.-Z. Shao and Z.-M. Su, *Chem. Commun.*, 2016, **52**, 9632-9635.
6. N. Ahmad, H. A. Younus, A. H. Chughtai and F. Verpoort, *Chem. Soc. Rev.*, 2015, **44**, 9-25.
7. H. Vardhan, M. Yusubov and F. Verpoort, *Coord. Chem. Rev.*, 2016, **306, Part 1**, 171-194.
8. M. J. Prakash and M. S. Lah, *Chem. Commun.*, 2009, DOI: 10.1039/B902988E, 3326-3341.
9. M. H. Alkordi, J. L. Belof, E. Rivera, L. Wojtas and M. Eddaoudi, *Chem. Sci.*, 2011, **2**, 1695-1705.
10. T. D. Hamilton, G. S. Papaefstathiou, T. Friščić, D.-K. Bučar and L. R. MacGillivray, *J. Am. Chem. Soc.*, 2008, **130**, 14366-14367.
11. J.-R. Li and H.-C. Zhou, *Nat. Chem.*, 2010, **2**, 893-898.
12. Y. Li, D. Zhang, F. Gai, X. Zhu, Y.-n. Guo, T. Ma, Y. Liu and Q. Huo, *Chem. Commun.*, 2012, **48**, 7946-7948.
13. L.-B. Sun, J.-R. Li, W. Lu, Z.-Y. Gu, Z. Luo and H.-C. Zhou, *J. Am. Chem. Soc.*, 2012, **134**, 15923-15928.
14. C. Wang, J. Shang, Y. Lan, T. Tian, H. Wang, X. Chen, J.-Y. Gu, J. Z. Liu, L.-J. Wan, W. Zhu and G. Li, *Adv. Funct. Mater.*, 2015, **25**, 6009-6017.
15. Y.-H. Kang, X.-D. Liu, N. Yan, Y. Jiang, X.-Q. Liu, L.-B. Sun and J.-R. Li, *J. Am. Chem. Soc.*, 2016, **138**, 6099-6102.
16. X. Qiu, W. Zhong, C. Bai and Y. Li, *J. Am. Chem. Soc.*, 2016, **138**, 1138-1141.
17. J.-R. Li, J. Yu, W. Lu, L.-B. Sun, J. Sculley, P. B. Balbuena and H.-C. Zhou, *Nat. Commun.*, 2013, **4**, 1538.
18. K. Wu, K. Li, Y.-J. Hou, M. Pan, L.-Y. Zhang, L. Chen and C.-Y. Su, *Nat. Commun.*, 2016, **7**, 10487.
19. D. Zhao, D. Yuan, R. Krishna, J. M. van Baten and H.-C. Zhou, *Chem. Commun.*, 2010, **46**, 7352-7354.
20. W. Lu, D. Yuan, A. Yakovenko and H.-C. Zhou, *Chem. Commun.*, 2011, **47**, 4968-4970.
21. D. Zhao, S. Tan, D. Yuan, W. Lu, Y. H. Rezenom, H. Jiang, L.-Q. Wang and H.-C. Zhou, *Adv. Mater.*, 2011, **23**, 90-93.
22. K. Sarkar, M. Paul and P. Dastidar, *Chem. Commun.*, 2016, **52**, 13124-13127.
23. J. Wang, C. He, P. Wu, J. Wang and C. Duan, *J. Am. Chem. Soc.*, 2011, **133**, 12402-12405.
24. L. Zhao, Y. Chu, C. He and C. Duan, *Chem. Commun.*, 2014, **50**, 3467-3469.
25. A. Cao, W. Zhu, J. Shang, J. H. Klootwijk, E. J. R. Sudhölter, J. Huskens and L. C. P. M. de Smet, *Nano Lett.*, 2016, DOI: 10.1021/acs.nanolett.6b02360.
26. M. Jung, H. Kim, K. Baek and K. Kim, *Angew. Chem. Int. Ed.*, 2008, **47**, 5755-5757.
27. Q.-G. Zhai, C. Mao, X. Zhao, Q. Lin, F. Bu, X. Chen, X. Bu and P. Feng, *Angew. Chem. Int. Ed.*, 2015, **54**, 7886-7890.
28. V. Brega, M. Zeller, Y. He, H. Peter Lu and J. K. Klosterman, *Chem. Commun.*, 2015, **51**, 5077-5080.
29. N. Hosono, M. Gochomori, R. Matsuda, H. Sato and S. Kitagawa, *J. Am. Chem. Soc.*, 2016, **138**, 6525-6531.
30. M. Han, R. Michel, B. He, Y.-S. Chen, D. Stalke, M. John and G. H. Clever, *Angew. Chem. Int. Ed.*, 2013, **52**, 1319-1323.
31. J. Park, L.-B. Sun, Y.-P. Chen, Z. Perry and H.-C. Zhou, *Angew. Chem. Int. Ed.*, 2014, **53**, 5842-5846.
32. J. W. Petr Klán, *Photochemistry of Organic Compounds: From Concepts to Practice*, Wiley, 2009.
33. V. Blanco, D. A. Leigh and V. Marcos, *Chem. Soc. Rev.*, 2015, **44**, 5341-5370.
34. A. J. Teator, D. N. Lastovickova and C. W. Bielawski, *Chem. Rev.*, 2016, **116**, 1969-1992.
35. T. R. Cook, Y.-R. Zheng and P. J. Stang, *Chem. Rev.*, 2013, **113**, 734-777.
36. T.-H. Chen, L. Wang, J. V. Trueblood, V. H. Grassian and S. M. Cohen, *J. Am. Chem. Soc.*, 2016, **138**, 9646-9654.
37. R. W. Larsen, *J. Am. Chem. Soc.*, 2008, **130**, 11246-11247.
38. L. Harmand, S. Cadet, B. Kauffmann, L. Scarpantonio, P. Batat, G. Jonusauskas, N. D. McClenaghan, D. Lastécouères and J.-M. Vincent, *Angew. Chem. Int. Ed.*, 2012, **51**, 7137-7141.
39. R. Beniazza, N. Bayo, F. Molton, C. Duboc, S. Massip, N. McClenaghan, D. Lastécouères and J.-M. Vincent, *Beilstein J. Org. Chem.*, 2015, **11**, 1950-1959.
40. B. J. Adzima, Y. Tao, C. J. Kloxin, C. A. DeForest, K. S. Anseth and C. N. Bowman, *Nat. Chem.*, 2011, **3**, 256-259.
41. L. Liang and D. Astruc, *Coord. Chem. Rev.*, 2011, **255**, 2933-2945.

View Article Online
DOI: 10.1039/C7CC04799A

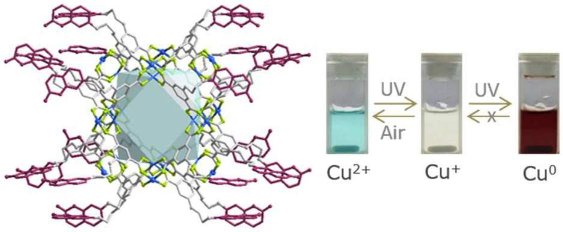

Controlled reduction of Cu^{2+} to Cu^{+}/Cu^{0} can be achieved by judicious ligand design in optically responsive metal-organic polyhedra systems.